thus focus on the coordinate part of phase space and much less on the role of momentum and kinetic energy.

The time scale of the energy fluctuation process (with the exception of vibrational energy, which is much longer) is seen to be ~250 fs. That it is so short can be understood by considering that in this particular reaction system, energy passes mainly through translational modes. As a general principle, the allowable time for the arising of a fluctuation will be limited by the time for its decay. For example, in our case a fluctuation producing translational excitation of nearby solvent atoms which occurred 5 ps before barrier climbing would not be useful, since the translational energy would have dissipated before it could be used for barrier climbing.

Acknowledgment. We thank J. T. Hynes, Antonio Liu, and John Rice for helpful dicussions. We also thank the National Science Foundation for supporting this work, both through research funds and a graduate fellowship to B.J.G.

Reaction-Surface Topography for Hydride Transfer: Ab Initio MO Studies of Isoelectronic Systems $CH_3O^- + CH_2O$ and $CH_3NH_2 + CH_2NH_2^+$

Ian H. Williams,*[1a] Andrea B. Miller,[1b] and Gerald M. Maggiora*[1b]

Contribution from Upjohn Company, Kalamazoo, Michigan 49001, and the School of Chemistry, University of Bristol, Bristol BS8 1TS, U.K. *Received May 17, 1989*

Abstract: The topography of the transition-state regions of the multidimensional potential energy surfaces for hydride transfer, (1) from methylamine to methaniminium and (2) from methoxide to formaldehyde, is described qualitatively on the basis of the characteristics (relative energies and curvatures) of critical points, each having negative curvature in the potential along the hydride-transfer reaction coordinate. Several new critical points on the HF/3-21G surfaces are reported. The geometry of hydride transfer depends upon steric effects, electrostatic interactions, and the possibility of 2e or 6e transition-state aromaticity. The varying interplay of these factors accounts for the differences between the reaction surfaces of the isoelectronic systems considered.

The simplest chemical reactions may be represented within the Born–Oppenheimer approximation by potential energy (PE) surfaces containing a reagent valley (or minimum) separated from a product valley (or minimum) by a saddle region associated with a transition state: the archetypal example of collinear $H + H_2$ springs readily to mind. Discussions of rates and mechanisms of organic reactions, involving polyatomic reagents, may acknowledge the multidimensional nature of the corresponding PE hypersurfaces but often implicitly assume a similarly simple picture for each elementary step. The degenerate hydride transfer $A'H^- + A \rightarrow A' + HA^-$ might be imagined as a simple process involving a unique saddle point (‡) located between the reagent and product valleys (R and P) represented schematically by the contours in the horizontal plane of Figure 1. If ‡ were the only critical point occurring in the vertical dividing plane describing bent symmetrical structures, then the simple picture would indeed be valid. In this paper we show, however, that a degenerate hydride transfer as "simple" as that with $A = A' = CH_2O$ may be suprisingly complex. The dividing hyperplane of symmetrical structures orthogonal to the hydride-transfer reaction coordinate (HTRC) contains many critical points within a chemically significant range of energies.

We have chosen the example of hydride transfer since this class of reaction has been the subject of numerous recent theoretical studies, owing to its importance in organic chemistry and biochemistry.[2-11] The PE hypersurface for degenerate hydride transfer from methylamine to the methaniminium cation (reaction 1)[7,10] has just two geometrically distinct critical points in the dividing hyperplane between reagents and products, but the corresponding hyperplane for the isoelectronic methoxide anion–formaldehyde system (reaction 2)[2,8,9] contains six geometrically distinct critical points in the range of chemical significance, only three of which have been reported previously. We now show how the critical points in these dividing hyperplanes may be organized topographically by consideration not only of their indices (the numbers of imaginary vibrational frequencies) but also importantly of the nature of the corresponding normal modes. This strategy for mapping the chemically relevant critical points of model (but real) chemical reaction surfaces is particularly useful when these surfaces are of a gently undulating nature; to follow an intrinsic reaction coordinate (IRC) over such an essentially flat surface is very difficult. The specific details of this topographical investigation may change at higher levels of theory (e.g., larger basis sets and/or inclusion of electron correlation), but it is not our present aim to provide a quantitatively accurate description of these energy surfaces or a complete account of the chemical

(1) (a) SERC Advanced Fellow, University of Bristol. Present address: School of Chemistry, University of Bath, Bath BA2 7AY, U.K. (b) Upjohn Co.

(2) Sheldon, J. C.; Bowie, J. H.; Hayes, R. N. *Nouv. J. Chim.* **1984**, *8*, 79.

(3) Donkersloot, M. C. A.; Buck, H. M. *J. Am. Chem. Soc.* **1981**, *103*, 6549; *Ibid.* **1981**, *103*, 6554. Brounts, R. H. A. M.; Buck, H. M. *Ibid.* **1983**, *105*, 1284.

(4) van der Kerk, S. M.; van Gerresheim, W.; Verhoeven, J. W. *Recl. Trav. Chim. Pays-Bas* **1984**, *103*, 143. Verhoeven, J. W.; van Gerresheim, W.; Martens, F. M.; van der Kerk, S. M. *Tetrahedron* **1986**, *42*, 975.

(5) Rzepa, H. S.; Miller, J. *J. Chem. Soc., Perkin Trans. 2* **1985**, 717. Rajyaguru, I. H.; Rzepa, H. S. *J. Chem. Soc., Chem. Commun.* **1987**, 998.

(6) Tapia, O.; Andres, J.; Aullo, J. M.; Bränden, C.-I. *J. Chem. Phys.* **1985**, *83*, 4673. Tapia, O.; Cardenas, R.; Andres, J.; Colonna-Cesari, F. *J. Am. Chem. Soc.* **1988**, *110*, 4046.

(7) Hutley, B. G.; Mountain, A. E.; Williams, I. H.; Maggiora, G. M.; Schowen, R. L. *J. Chem. Soc., Chem. Commun.* **1986**, *267*; *Ibid.* 1303.

(8) Wu, Y.-D.; Houk, K. N. *J. Am. Chem. Soc.* **1987**, *109*, 906.

(9) Field, M. J.; Hillier, I. H.; Smith, S.; Vincent, M. A.; Mason, S. C.; Whittleton, S. N.; Watt, C. I. F.; Guest, M. F. *J. Chem. Soc., Chem. Commun.* **1987**, 84. Hillier, I. H.; Smith, S.; Mason, S. C.; Whittleton, S. N.; Watt, C. I. F.; Willis, J. *J. Chem. Soc., Perkin Trans. 2* **1988**, 1345.

(10) Wu, Y.-D.; Houk, K. N. *J. Am. Chem. Soc.* **1987**, *109*, 2226.

(11) Pain, A. E.; Williams, I. H. *J. Chem. Soc., Chem. Commun.* **1988**, 1367. Pain, A. E.; Williams, I. H. Manuscript in preparation.

0002-7863/90/1512-530$02.50/0

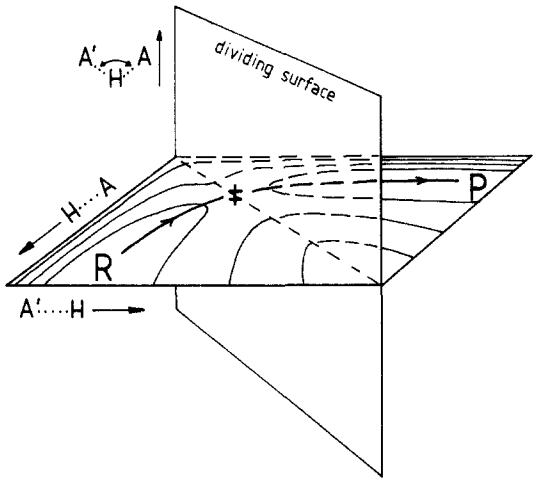

Figure 1. Schematic energy contours in horizontal plane for (collinear) hydride transfer $A'H^- + A \rightarrow A' + HA^-$ and vertical plane representing bent structures orthogonal to the asymmetric A'···H···A stretching reaction coordinate.

Table I. Total Energies (Hartrees) and Symmetries for HF/3-21G Optimized Structures and Indices of Corresponding Critical Points on PE Hypersurfaces

species	pt gp	total energy	index
$CH_2NH_2^+$	C_{2v}	-93.862 84	0
CH_3NH_2	C_s	-94.681 66	0
1	C_{2v}	-188.534 26	1
2	C_{2h}	-188.529 63	2
3	D_{2d}	-188.394 29	4
4	D_{2h}	-188.142 67	6
CH_3O^-	C_{3v}	-113.724 80	0
CH_2O	C_{2v}	-133.221 82	0
5	C_{2v}	-226.929 16	1
6	C_{2v}	-226.928 88	2
7	C_{2v}	-226.934 12	2
8	C_{2h}	-226.939 67	3
9	C_2	-226.939 70	2
10	C_s	-226.941 95	1

mechanisms. Instead, our purpose here is to demonstrate the general features of the transition-state regions of the PE hypersurfaces for a pair of isoelectronic reacting system—their similarities and differences—as described by a particular theoretical model. Detailed studies[11] of the topography of PE surfaces for reaction 3 at various levels of ab initio theory have demonstrated

$$CH_3NH_2 + CH_2{=}NH_2^+ \rightarrow CH_2{=}NH_2^+ + CH_3NH_2 \quad (1)$$

$$CH_3O^- + CH_2{=}O \rightarrow CH_2{=}O + CH_3O^- \quad (2)$$

$$CH_2{=}NH + CH{\equiv}NH^+ \rightarrow CH{\equiv}NH^+ + CH_2{=}NH \quad (3)$$

that the qualitative features determined at the HF/3-21G level are the same as those at the MP2/6-311G** level; i.e., the index of each critical point remains unaltered. It therefore seems likely that the major topographical features of the PE surfaces described in this work on the basis of HF/3-21G calculations would persist at higher levels of theory, although the details of relative energetics and curvatures would differ somewhat.

Methods and Results

Geometry optimizations and saddle-point searches at the HF/3-21G level of molecular orbital theory were performed with the CADPAC program[12] by Schlegel's method.[13] Diffuse basis functions, which would be essential for accurate results on the anionic surface, were not included in this study. Cartesian force constants computed analytically within CADPAC program,[14] to characterize each critical point. Intrinsic reaction coordinates[15] were determined, with the GAMESS program,[16] from each saddle point in each direction of negative curvature of the PE hypersurface to verify the pathways between the various critical points.

Tables I and II, respectively, contain the HF/3-21G total energies and optimized geometries for the reagents and transition structures (TSs) **1–10** illustrated in Figure 2. As discussed below, the in-plane (σ) orbitals of **1** and **5** involved in the bond making and breaking are isoconjugate with the π-orbitals of the cyclopentadienyl anion. These five molecular orbitals are sketched schematically in Figure 3 together with the corresponding orbitals for **2** and **8**; the HOMO and LUMO are indicated, and the orbital energies and symmetries are also given. Although in each case

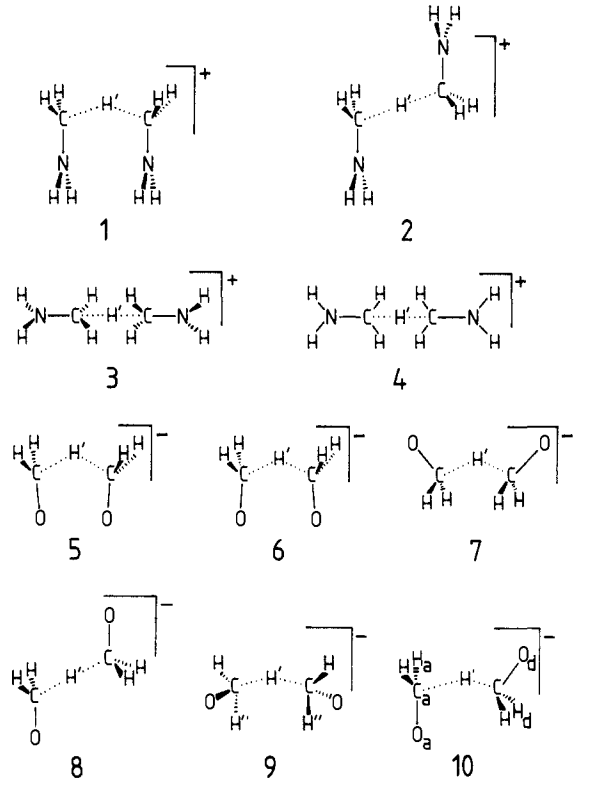

Figure 2. Critical points **1–10**.

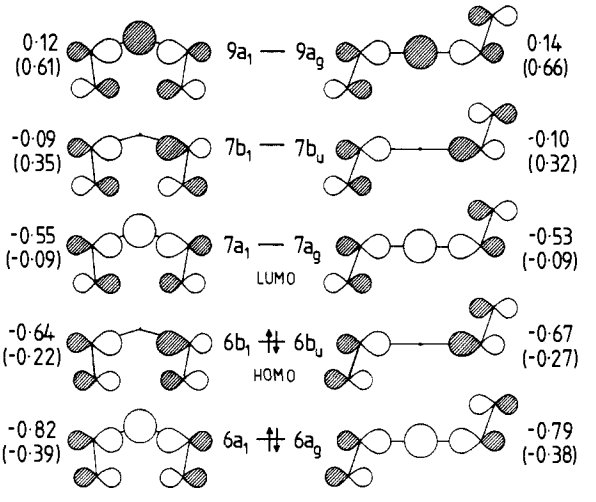

Figure 3. Selected in-plane molecular orbitals involving making and breaking bonds for C_{2h} and C_{2v} transition structures. For the quasi-cyclic V-shaped C_{2v} structures **1** and **5** these five are analogous to the π molecular orbitals of cyclopentadienyl anion. Atomic lobes are not drawn to scale: the carbon coefficients in the HOMOs are actually close to zero. Orbital energies for $CH_3NH_2/CH_2NH_2^+$ and (in parentheses) for CH_3O^-/CH_2O are given in hartrees.

(12) Amos, R. D. CADPAC, Version 3.0; University of Cambridge: Cambridge, England, 1986.
(13) Schlegel, H. B. *J. Comput. Chem.* **1982**, *3*, 214.
(14) Williams, I. H. Unpublished work.
(15) Schmidt, M. W.; Gordon, M. S.; Dupuis, M. *J. Am. Chem. Soc.* **1985**, *107*, 2585.
(16) Schmidt, M. W.; Boatz, J. A.; Baldridge, K. K.; Koseki, S.; Gordon, M. S.; Elbert, S. T.; Lam, B. *QCPE* **1987**, *7*, 115.

Table II. HF/3-21G Optimized Geometries

(a) $CH_3NH_2/CH_2NH_2^+$ Species[a]

	$CH_2NH_2^+$	CH_3NH_2	**1**	**2**	**3**	**4**
CN	1.268	1.471	1.345	1.347	1.275	1.347
CH′		1.090	1.322	1.318	2.505	1.345
CH	1.072	1.082	1.076	1.077	1.073	1.077
NH	1.010	1.003	0.999	0.999	1.006	0.998
CH′C			154.3	180.0	180.0	180.0
NCH′		114.8	108.6	111.7	180.0	180.0
H′CH		108.9	97.9	96.9	56.1	67.9
CNH	122.2	113.6	121.4	121.5	122.1	121.3
NH′CH		±120.9	±121.8	±122.1		
H′CNH		±64.0	±93.3	±89.7		

(b) CH_3O^-/CH_2O Species[a]

	CH_3O^-	CH_2O	**5**	**6**	**7**	**8**	**9**[b]	**10**[c]
CO	1.348	1.207	1.258	1.261	1.261	1.270	1.270	1.278, 1.25
CH′	1.134		1.420	1.405	1.463	1.393	1.390	1.346, 1.55
CH	1.134	1.083	1.103	1.104	1.102	1.101	1.102, 1.100	1.106, 1.09
CH′C			139.2	148.5	151.3	180.0	173.3	133.8
OCH′	117.3		111.9	113.9	118.1	115.4	115.3	117.7, 109
H′CH	100.6		93.3	92.8	90.5	92.1	92.6, 91.6	92.3, 91.0
OH′CH			±125.6	±125.8	±125.6	±125.7	125.6, −125.7	±127.1, ±124

[a] Bond lengths in angstroms, angles in degrees. [b] The first value of a pair refers to H and the second to H″ (see Figure 1). The dihedral angle CH′CO = 78.9°. [c] The first value of a pair refers to the hydride donor (e.g., $O_dC_dH_d$ in Figure 1) and the second to the hydride acceptor (e.g., $O_aC_aH_a$ in Figure 1).

Table III. Unscaled HF/3-21G Vibrational Wavenumbers (cm^{-1}) and Assignments for Normal Modes of C_{2h} and V-Shaped C_{2v} Transition Structures

C_{2v}				C_{2h}			
assignment[a]	mode[b]	**1**	**5**	**2**	**8**	mode[b]	assignment[a]
asym CH′, b_1	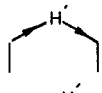	1060*i*	1119*i*	1048*i*	1191*i*	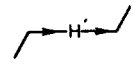	asym CH′, b_u
C_2 torsion, a_2	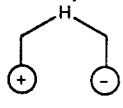	101	111	24*i*	26*i*	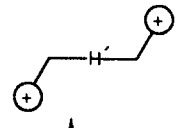	CH′C torsion, a_u
C_s torsion, b_2	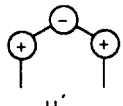	354	346	89	60*i*	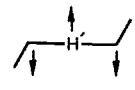	CH′C ip, b_u
sym CH′, a_1	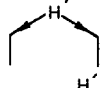	511	403	266	197	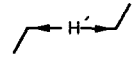	sym CH′, a_g
CH′C ip, a_1	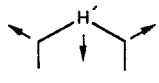	200	130	329	306	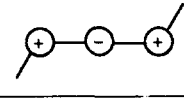	CH′C op, a_u

[a] Asym and sym are antisymmetric and symmetric stretching modes, respectively; ip and op refer to in-plane and out-of-plane bending modes, respectively. [b] Arrows indicate the relative atomic motions dominating each normal mode; + and − indicate upward and downward motions, respectively.

Table IV. Unscaled HF/3-21G Vibrational Wavenumbers (cm^{-1}) and Assignments for Critical Points on the CH_3O^-/CH_2O PE Hypersurface

		C_{2v}		C_2			C_s			
assignment[a]		**5**	**6**	**7**		**9**	**8**	**10**		assignment[a]
asym CH′ str	(b_1)	1119*i*	1161*i*	1308*i*	(b)	1183*i*	1191*i*	1049*i*	(a′)	asym CH′ str
C_2 torsion	(a_2)	111	50	96*i*	(a)	35	26*i*	22	(a″)	CH′C torsion
CH′C ip bend	(a_1)	130	100*i*	88	(a)	179	60*i*	313	(a″)	CH′C op bend
sym CH′ str	(a_1)	403	363	215	(a)	305	197	298	(a′)	sym CH′ str
C_s torsion	(b_2)	346	312	280	(b)	80*i*	306	165	(a′)	CHC ip bend

[a] See footnote to Table III.

the HOMO and LUMO are orbitals 17 and 18 in the canonical ordering, the other three orbitals are not consecutive with these. Assignments and wavenumbers for five of the low-frequency vibrational modes of **1**, **2**, **5**, and **8** are given in Table III: these are the modes of greatest interest in regard to understanding the topographical features of the surfaces discussed below. Similar information for the same five modes of **5**–**10** inclusive is presented in Table IV in such a way as to facilitate their comparison.

Figure 4 shows charge distributions for **1**, **2**, **5**, and **8** obtained from the wave functions by distributed multipole analysis[17] (DMA), as available within CADPAC, using atomic multipole sites. Only the point-charge and point-dipole values are shown. The point charges indicate CX bond polarity (X = N or O) in the sense C^+X^- (reflecting the dif-

(17) Stone, A. J. *Chem. Phys. Lett.* **1981**, *83*, 233.

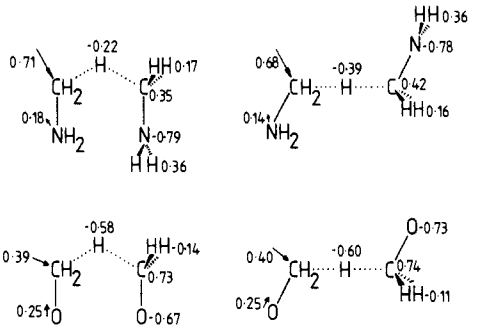

Figure 4. Distributed multipole analyses (in atomic units) for C_{2v} and C_{2h} transition structures. Point dipoles (left-hand side, arrows point toward negative charge) and point charges (right-hand side) are computed for atomic centers (1 au = 2.54 D for dipole moments).

ference in electronegativity), whereas the point dipoles indicate bond polarity in the opposite sense C^-X^+. This partial compensation of point-charge and point-dipole contributions for CN bonds has been noted previously.[18]

Strategy for Topographical Exploration

According to the symmetry rules of Stanton amd McIver,[19] the reaction-coordinate vibrational mode for a TS (the transition vector) must be antisymmetric for any symmetry operation that interconverts the reagents and products. It is commonly held that this implies that the TS for a degenerate reaction (such as reaction 1 or 2) must itself be symmetric and may be located by constrained-geometry optimization within the subspace of coordinates belonging to the totally symmetric irreducible representation.[20] This inference is incorrect, for it presupposes the presence of a symmetry operation interconverting reagents and products; it does not provide a sufficient criterion for TS location by a simple energy-minimization technique. What this particular Stanton–McIver symmetry rule does imply is that *if* there exists a symmetrical TS (i.e., one possessing a symmetry element whose operation interconverts reagents and products), *then* the transition vector must belong to some irreducible representation other than the totally symmetric one. As such, this rule is useful in that it does suggest a rational strategy for organizing the topographical features of a PE hypersurface for a symmetrical process. The following discussion complements Schlegel's reviews of TS-optimization techniques.[20,21]

To begin with, chemical intuition should be employed to suggest a small number of high-symmetry structures as initial candidates for TSs. This number should certainly include those structures that satisfy the usual rules of valency and stereochemistry, but it should not be restricted by lack of imagination. Each of these candidates in turn is then subjected to constrained-geometry optimization within its symmetry point group to locate the nearest critical point. It is well-known that gradient-based optimization methods are symmetry preserving: hence, the minimum energy structure located in this step possesses the same (or possibily higher, but not lower) symmetry as the starting structure. Moreover, a critical point in the subspace of the totally symmetric irreducible representation is also a critical point in the full coordinate space of the system, but its index may change between the subspace and the full space. Thus, a minimum (index 0) located in a constrained optimization may prove to be a first or higher order saddle point (index ≥ 1) on the full PE hypersurface. It is essential therefore to characterize the critical point by determination of its curvatures; this is indeed recommended practice.[20,21] However, we emphasize here the importance of considering not only the eigenvalues of the matrix of second derivatives of the energy but also its eigenvectors—in particular any transition vectors.

The normal modes should be inspected to identify possible paths interconnecting the known critical points, and hypotheses concerning their organization may be proposed. For example, the simplest hypothesis concerning the path between a minimum and a nearby saddle point of higher energy is that there are no additional critical points separating them (provided that the transition vector is appropriate to reach this minimum); this hypothesis may be tested by application of a reaction path following algorithm starting from the saddle point along the transition vector. If the transition vector does not lead toward the minimum in question, then *as far as the path interconnecting them is concerned*, these two critical points are both minima. In this case it is reasonable to suppose that a saddle point separates them. The simplest hypothesis concerning two adjacent saddle points whose transition vectors are correlated is that there is an intervening minimum. The nature of the search for a critical point along a path depends upon the inferred index of that critical point and on the symmetry of the path. A minimum may, of course, be located by energy minimization within the appropriate symmetry constraint. A saddle point may be located by energy minimization provided that its transition vector does not belong to the totally symmetric irreducible representation; otherwise, it must be located by a saddle-point searching algorithm.

Analysis of PE Surface Curvature: Second-Order Jahn–Teller Effect. The second-order Jahn–Teller (SOJT) effect[22] affords a suitable means for *qualitatively* examining the electronic factors responsible for PE hypersurface curvature, which is particularly important in regions in the neighborhood of critical points where the slope of the hypersurface is zero. In the present work, the SOJT effect is shown to provide a basis for analyzing PE hypersurface features for reactions 1 and 2, in critical point regions of chemical interest.

From quantum mechanical perturbation theory it follows that the curvature of a PE hypersurface with respect to the coordinate Q is given by[22]

$$\frac{\partial^2 E}{\partial Q^2} = \left\langle \psi_0 \left| \frac{\partial^2 V_{ne}}{\partial Q^2} + \frac{\partial^2 V_{nn}}{\partial Q^2} \right| \psi_0 \right\rangle + \sum_{i \geq 1} \frac{\left| \left\langle \psi_0 \left| \frac{\partial V_{ne}}{\partial Q} \right| \psi_k \right\rangle \right|^2}{E_0 - E_k} \quad (4)$$

where E, V_{ne}, and V_{nn} are the total, nuclear–electron, and nuclear–nuclear energies, respectively, and the ψ's represent the wave functions for the ground, ψ_0, and excited, $\psi_1, \psi_2, \ldots, \psi_k, \ldots$, electronic states. As the first term in eq 4 is always positive, it follows that the magnitude of the second, or response term, relative to the first term determines the sign of the curvature along Q.

In the present work the coordinates of interest will generally not include the true reaction coordinate Q_r, but rather coordinates that move the system toward critical points away from the current one (cf. Figures 5, 6, and 8). The symmetry of each of the coordinates is denoted by an appropriate irreducible representation of the point group corresponding to the current critical point, and is given in Tables III and IV.

To apply the SOJT effect approach qualitatively, it is necessary first to determine whether the integral $\langle \psi_0 | \partial V_{ne}/\partial Q | \psi_k \rangle$ in the response term given in eq 4 is zero or nonzero and second to make some estimate of its magnitude relative to the first term. While the latter is most difficult to determine (cf. ref 22b), the former can be determined by symmetry considerations alone. In this regard, the symmetry properties of the terms in $\langle \psi_0 | \partial V_{ne}/\partial Q | \psi_k \rangle$ must be examined: (a) $\partial V_{ne}/\partial Q$ has the same symmetry ("transforms") as Q (see Tables III and IV) and (b) the symmetry of the wave function product $\psi_0 \psi_k$ must be the same as that of $\partial V_{ne}/\partial Q$ for the integral to be nonzero. If it is assumed that the excited-state wave functions can be approximated by single, singly excited configurations, then the wave function product is ap-

(18) Price, S. L.; Stone, A. J. *Chem. Phys. Lett.* **1983**, *98*, 419.
(19) Stanton, R. E.; McIver, J. W. *J. Am. Chem. Soc.* **1975**, *97*, 3632.
(20) Schlegel, H. B. In *New Theoretical Concepts for Understanding Organic Reactions*; Bertrán, J., Csizmadia, I. G., Eds.; Kluwer Academic Publishers: Dordrecht, 1989.
(21) Schlegel, H. B. *Adv. Chem. Phys.* **1987**, *67*, 249.
(22) (a) Pearson, R. G. *Symmetry Rules for Chemical reactions*; Wiley: New York, 1976. (b) Simons, J. *Energetic Principles of Chemical Reactions*; Jones and Barlett: Boston, 1983. (c) Salem, L. *Electrons in Chemical Reactions: First Principles*; Wiley: New York, 1976.

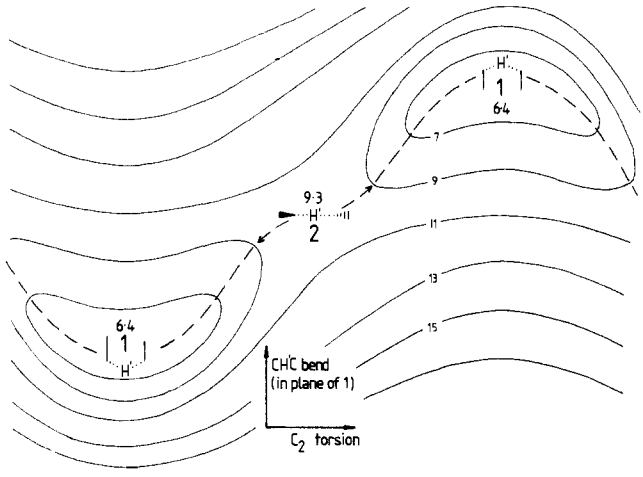

Figure 5. Schematic contour map of $CH_3NH_2/CH_2NH_2^+$ critical points orthogonal to the hydride-transfer reaction coordinate. Energies in kilocalories per mole.

proximately given by the MO product $\phi_i\phi_{i'}$, where ϕ_i and $\phi_{i'}$ are the appropriate occupied and unoccupied orbitals. In this case, the symmetry of $\psi_0\psi_k$ is identical with that of $\phi_i\phi_{i'}$. The symmetries of the relevant frontier orbitals are given in Figure 3.

Discussion

Methylamine/Methaniminium. Figure 5 is a schematic representation of a projection onto two dimensions of the 32-dimensional hyperplane of symmetrical structures orthogonal to the HTRC mode for reaction 1. The two dimensions selected are the two valence coordinates that dominate the pathway interconnecting the critical points of interest in the hyperplane. Each point on the contour diagram of Figure 5 is orthogonal to the HTRC; the full hypersurface (in the space of 33 internal degrees of freedom and with potential energy as the ordinate) has negative curvature in the potential along this direction at each point in the figure. The true index of each critical point in the figure is therefore greater by 1 than its apparent index: the apparent minimum labeled as **1** is actually a first-order saddle point, and the apparent saddle point labeled as **2** is actually a second-order saddle point.

A feasible candidate for a $CH_3NH_2/CH_2NH_2^+$ TS is C_{2h} structure **2**, which proves to be a second-order saddle point. Besides the HTRC mode, there is negative curvature in the potential along the CH'C torsional mode; displacement in this coordinate reduces the symmetry from C_{2h} to C_2. Careful optimization[23] within C_2 symmetry leads directly to V-shaped C_{2v} structure **1**, which is a first-order saddle point; this is the only true TS for hydride transfer.[10]

The negative curvature of the potential along the HTRC at each critical point may be understood as a consequence of a SOJT effect (vide supra). The asymmetric CH stretching vibrational mode has the same symmetry (b_1 in C_{2v}, b_u in C_{2h}) as the low-lying excited state generated by promotion of a single electron from the HOMO to the LUMO; distortion in this coordinate therefore permits an energetically favorable change in the electronic wave function through mixing with this excited state. It is not possible, however, to rationalize similarly the negative curvature of the potential possessed by the C_{2h} second-order TS **2** in the a_u-symmetrical CH'C torsional mode also. There is an energetically feasible single excitation from each of the four highest double-occupied MOs, each leading to a configuration with the appropriate a_u symmetry, and consideration of the four corresponding excitations of **1** does not reveal any obvious difference that might account for why the torsional mode concerned has a wavenumber of 101 cm^{-1} in **1** but of 24*i* cm^{-1} in **2**. Differences in curvature of this small magnitude are presumably too subtle to be explicable by a simplified SOJT approach on the basis of consideration of the symmetries of only the frontier orbitals.

The stability of **1** relative to **2** may be regarded as a consequence of transition-state aromaticity. Wu and Houk[10] have alluded to a pericyclic component to hydride transfer and have discussed qualitatively the stabilizing features of the HOMO for **1**. An aromatic C_{2v} transition structure for degenerate hydride transfer from methylimine to formonitrilium cation (reaction 3) optimized at the MP2/6-311G** level has recently been reported;[11] this system is stereoelectronically better defined than the present $CH_3NH_2/CH_2NH_2^+$ system. The quasi-cyclic C_{2v} structure, with each nitrogen lone pair synperiplanar with the transferring hydride, was calculated to be ~16 kcal mol^{-1} more stable than the corresponding acyclic C_{2h} structure. The lone pairs on each nitrogen, together with the electron pair formally associated with the transferring hydride, constitute a Hückel aromatic sextet: the in-plane (σ) orbitals involved in bond making and breaking are isoconjugate with the π-orbitals of cyclopentadienyl anion, another 5-center, 6-electron system with Hückel topology. The magnitude of the aromatic stabilization (the energetic difference between the acyclic and cyclic structures) depends crucially upon the geometry of the quasi-cyclic species: the shorter the nonbonded N···N distance, the greater the stabilization.[11] The same trend may be discerned from the data reported by Wu and Houk:[10] at the HF/3-21G level, the optimum N···N distance is 2.905 Å in **1**, which is 2.9 kcal mol^{-1} lower in energy than **2**, but at the MP2/6-31G* level, the N···N distance is only 2.633 Å and the aromatic stabilization is 5.7 kcal mol^{-1}.

If hydride was transferred strictly as H^- with 2 electrons, the expected charge distribution (iminium:hydride:iminium) in the TS would be +1:−1:+1. The DMA of the electronic charge distribution for **2** (Figure 4) suggests that the actual charges are more like +0.69:−0.38:+0.69. Similarly, the DMA for **1** (Figure 4) shows even less accentuated charges, viz. +0.61:−0.22:+0.61. The difference between the charge distributions of **1** and **2** is due mainly to redistribution between the hydride and the methylene groups, since the charges on the amine groups are essentially the same (and rather small). We have found a critical point on the energy hypersurface at which the DMA reveals almost unit charges of +0.96:−0.92:+0.96. This species (**3**) has D_{2d} symmetry, has very long (2.505 Å) CH' bonds, and is at a minimum with respect to hydride transfer, despite being 94 kcal mol^{-1} higher in energy than the reagents. It is a fourth-order saddle point with negative curvatures in the potential for distortions along two pairs of degenerate linear bending modes. Twisting one of the iminium moieties through 90° yields a planar D_{2h}-symmetrical species (**4**) with short (1.345-Å) CH' bonds, lying 252 kcal mol^{-1} above the reagents. This is a sixth-order saddle point; besides being at a maximum with respect to torsional motion about the molecular axis, it is also now a TS for hydride transfer. However, the DMA shows the charge distribution to be +0.31:+0.38:+0.31; i.e., there is no hint of hydridic character whatsoever. The details of these charge distributions are liable to depend upon the nature of the basis set used; in particular the lack of diffuse functions on the transferring hydrogen in this study may tend to underestimate its negative charge somewhat.

Methoxide/Formaldehyde. Figure 6a is a schematic representation of the two-dimensional projection map of symmetrical structures orthogonal to the HTRC for reaction 2. The two dimensions are the C_2-axis-conserving torsional coordinate and the CH'C bending coordinate in the plane of the C and O atoms of **5**; this choice corresponds to the pair used to construct Figure 5 for the isoelectronic $CH_3NH_2/CH_2NH_2^+$ system. Comparison of Figures 5 and 6a is perhaps startling. In each case the C_{2h} and V-shaped C_{2v} structures are critical points (and are drawn in equivalent locations in the two figures to facilitate comparison), and in each case the projection map indicates a portion of a zigzag-shaped valley. These valleys run east–west between steeply rising walls to north and south, and their floors are gently undulating. However, whereas the valley in Figure 5 runs northeast to southwest and passes directly from one C_{2v} structure to its mirror

(23) Optimization within C_2 symmetry starting from a substantially bent geometry (CH'C ~120°), but with essentially antiperiplanar NOCN atoms, yields a species with almost collinear CH'C atoms (178.9°) and an NOCN dihedral angle of ~170°. This species is of lower energy than C_{2h} structure **2** and satisfies the usual criteria for an optimized geometry but is not a critical point!

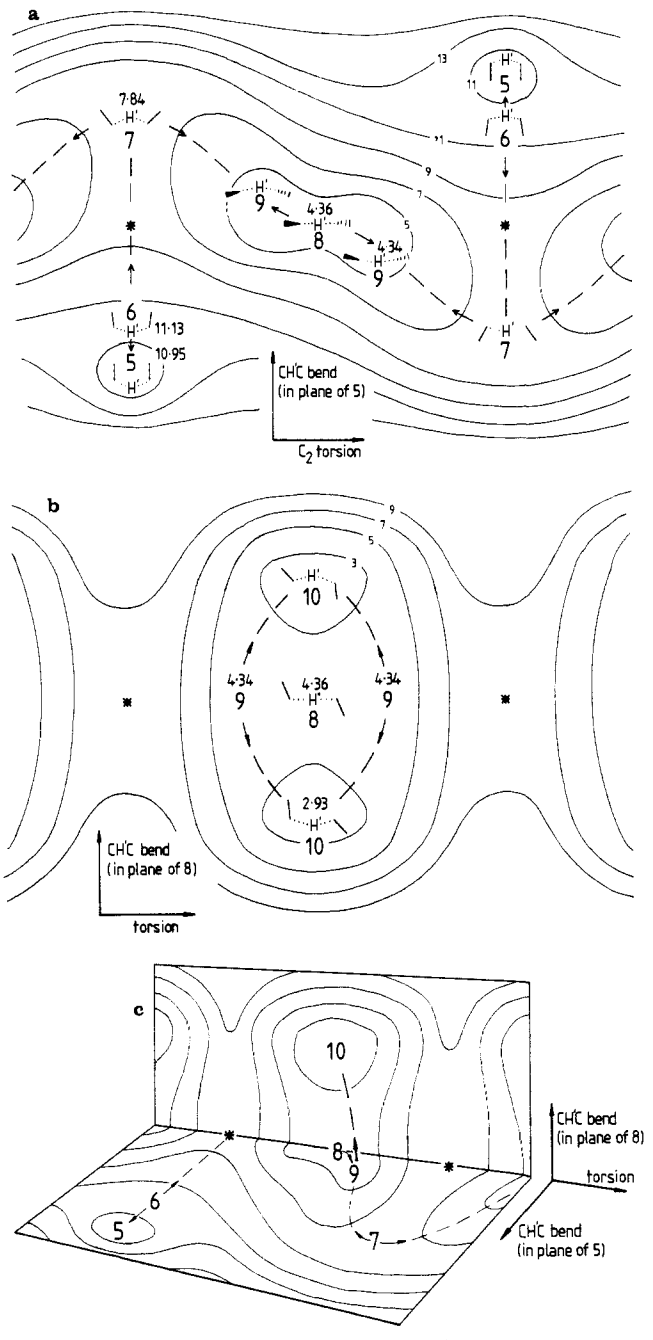

Figure 6. Schematic contour maps of CH_3O^-/CH_2O critical points orthogonal to the hydride-transfer reaction coordinate: (a) projected onto the plane defined by the C_2-axis-conserving torsional coordinate and the in-plane CH'C bending coordinate of **5** (i.e., the same plane as Figure 5); (b) projected onto the plane defined by the CH'C torsion (no longer C_2-axis-conserving) and the in-plane CH'C bending coordinate of **8**; (c) showing the perpendicular relationship between (a) and (b).

image by means of the C_{2h} saddle point, the valley in Figure 6a runs southeast to northwest and does *not* pass through the V-shaped C_{2v} structures. This latter species **5** remains a first-order saddle point on the CH_3O^-/CH_2O PE hypersurface, corresponding to a minimum on Figure 6a, but it is no longer the lowest energy TS. Instead it occupies a shallow corrie set in the valley wall. To proceed northward from the southwest corrie of Figure 6a corresponds to an in-plane CH'C bending motion that conserves C_{2v} symmetry. Opening this angle from 139° by only 10° leads to the second-order saddle point **6** only 0.2 kcal mol^{-1} above **5**. Passage over this shallow lip then leads down a ridge to another second-order saddle point **7**; this point is at a minimum in the CH'C bending coordinate (in C_{2v} symmetry) but is at a maximum in the C_2-axis-conserving torsional coordinate and lies on the path running along the main valley floor. The structure at this point is W-shaped: the CH'C bending coordinate has passed through linearity and now adopts an angle of 151°. This structure **7** has been reported by Wu and Houk[8] and by Hillier and co-workers.[9] Note that there are two second-order saddle points with C_{2v} symmetry, **6** and **7**, which may be distinguished by inspection of their transition vectors (see above).

Structure **8** (cf. ref 2) is, surprisingly, a third-order saddle point (as noted by Wu and Houk[8]). The imaginary vibrational wavenumber for the CH'C torsional mode is 26*i* cm^{-1} as compared with 24*i* cm^{-1} for **2** (Table III). A distortion away from C_{2h} symmetry along this normal mode for **2** on the $CH_3NH_2/CH_2NH_2^+$ surface *does not* lead to any nearby critical point of C_2 symmetry but only to C_{2v} structure **1** via a 180° rotation in the dihedral angle. However, just such a C_2-symmetrical distortion away from **8** on the CH_3O^-/CH_2O surface *does* lead to a proximate critical point: a dihedral angle change of only ~22° leads to the second-order saddle point **9**, with a CH–C angle of 173°, only 0.02 kcal mol^{-1} lower than **8**. But this is not the lowest energy hydride-transfer TS, despite being the lowest energy species depicted on Figure 6a. Displacement in the in-plane bending mode of **8** with negative curvature (60*i* cm^{-1}) lowers the symmetry to C_s, and in this point group the HTRC now belongs to the totally symmetric irreducible representation. Hence, the first-order hydride-transfer TS **10** (cf. ref 8) may *not* be located by energy minimization within the C_s-symmetrical subspace, despite the fact that it is a TS for a symmetric exchange reaction; it may be found by a saddle point search in C_s symmetry. The overall symmetry of the degenerate reaction 2, however, requires the existence of an identical C_s-symmetrical TS on the other side of the local C_{2h}-symmetrical maximum. Just as **10** is an example of an asymmetrical TS for a degenerate reaction, so also the fact that structure **3** for $CH_3NH_2/CH_2NH_2^+$ system is at a local minimum with respect to the HTRC further demonstrates the falsity of the proposition that the TS for a degenerate reaction must itself be symmetric.

Figure 6b shows a projection of the hypersurface onto the two-dimensional plane described by the CH'C in-plane bend of **8** and the CH'C torsion (no longer a C_2-axis-conserving coordinate in this plane), and Figure 6c shows how the planes of Figure 6a, are perpendicularly related. The points marked by an asterisk in Figure 6b appear to be saddle points for internal rotation of **8** about the collinear CH'C axis; however, the gradient in the CH'C angle bending coordinate is not zero, so these are not critical points on the full hypersurface. The same structure, with collinear CH'C atoms, is traversed on the pathway between **6** and **7**, as shown in Figure 6a.

The existence of negative curvature in the potential along the HTRC may again be understood as a SOJT effect: distortion in the b_u CH'C stretching mode permits an energetically favorable mixing with the low-lying excited state of the same symmetry (corresponding to a HOMO–LUMO excitation). However, CH'C bending in the plane of the C and O atoms of **8** (the plane of Figure 6b) is also a vibrational mode of b_u symmetry, and distortion in this coordinate also permits the same mixing of states, but less effectively than the asymmetric stretching mode. Nonetheless, the stabilization accompanying this bending distortion of **8** outweighs the restoring force due to steric interactions, and leads to negative curvature in the potential along this coordinate (vibrational wavenumber 60*i* cm^{-1}). For the case of $CH_3NH_2/CH_2NH_2^+$, the steric interactions accompanying this b_u CH'C bending distortion of **2** are greater (since the motion tends to bring together the hydrogen atoms of distal amino and methylene groups), and are not outweighed by the SOJT stabilization: the curvature of the potential along this coordinate is small and positive (vibrational wavenumber 89 cm^{-1}).

Factors Influencing Hydride-Transfer Geometry. A triangular CH'C arrangement would, as pointed out by Lewis and Symons,[24] be the natural consequence of attack by the electrophilic hydride acceptor upon the electron density of the CH' bond of the hydride donor. A preference for a bent geometry may also be predicted

(24) Lewis, E. S.; Symons, M. C. R. *Q. Rev. Chem. Soc.* **1958**, *12*, 230.

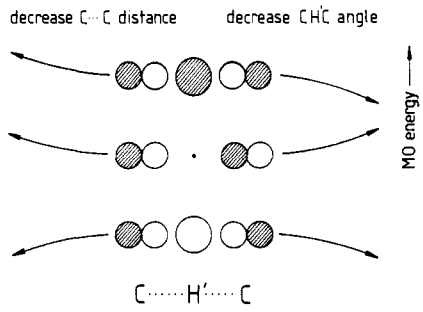

Figure 7. Walsh diagram indicating trends in orbital energy changes for simplified 3-center C···H'···C system as a function of decreasing C···C distance (left-hand side) and decreasing CH'C angle (right-hand side). For hydride transfer (involving two electrons), the lowest orbital is the HOMO. For proton transfer (involving four electrons), the second orbital is the HOMO and all predictions are reversed.

from a simple Walsh diagram (Figure 7): Swain et al.[25] argued in this manner that hydride transfer (two electrons in the three fragment MOs of Figure 7) would prefer *shorter* CH' bonds, whereas Olah et al.[26] have noted the increased bonding overlap that accompanies angle bending in the general 3-center 2-electron case. However, the counteracting tendency of steric interactions has also long been recognized,[27] and the possible role of electrostatic interactions has been suggested.[10] In our opinion these three factors are sufficient to account for the geometrical variety of hydride-transfer transition structures on the isoelectronic $CH_3NH_2/CH_2NH_2^+$ and CH_3O^-/CH_2O hypersurfaces, provided that the concept of stabilization for bent CH'C geometries *is* extended to include not only the 3-center 2-electron case (isoconjugate with cyclopropenium cation) but also the 5-center 6-electron case (isoconjugate with cyclopentadienyl anion) that may occur when the hydride donor and acceptor carbon atoms each bear a heteroatom substituent, e.g., NH_2 or O. These ideas are further discussed elsewhere.[28]

Structure **1** is stabilized by 5-center 6-electron bonding (6e TS aromaticity), offset by small steric and electrostatic repulsive contributions. Distortion away from this geometry diminishes the stabilizing interaction, and this diminution is most marked for distortions that reduce the overlap between the nitrogen lone-pair orbitals. A C_2-axis-conserving torsional motion necessarily destroys the 5-center 6-electron stabilization but allows the (weaker) 3-center 2-electron stabilization (2e TS aromaticity) to remain, initially at least; as structure **2** is approached, the steric and electrostatic factors are favorable but all trace of TS aromaticity is lost in the linear CH'C geometry. Distortion of **1** by CH'C bending means loss of both 6e and 2e TS aromaticity simultaneously; this is accompanied by a steeper initial rise in energy, which is later augmented by unfavorable steric interactions between the methylene groups in **7**. The sum of the DMA atomic charges (Figure 4) for each NH_2 group of **1** is only −0.07, so the Coulombic repulsion between them is small.

In contrast, the 6e TS aromaticity of **5** is almost entirely outweighed by unfavorable Coulombic interactions between the oxygen atoms, each of which bears a charge of −0.67 according to the DMA (Figure 4). (The changes in the DMA atomic dipoles as between the V-shaped C_{2v} and the C_{2h} structures, however, are similar for both the CH_3O^-/CH_2O and $CH_3NH_2/CH_2NH_2^+$ cases.) The repulsive electrostatic interactions are relieved in **7**, but this is unstable with respect to torsional distortion, owing to unfavorable steric interactions between the methylene groups. Although **8** is sterically and electrostatically favorable, it is locally unfavorable since either of two b_u vibrational modes allows the CH'C coordinate to adopt a bent geometry (C_2 or C_s symmetry)

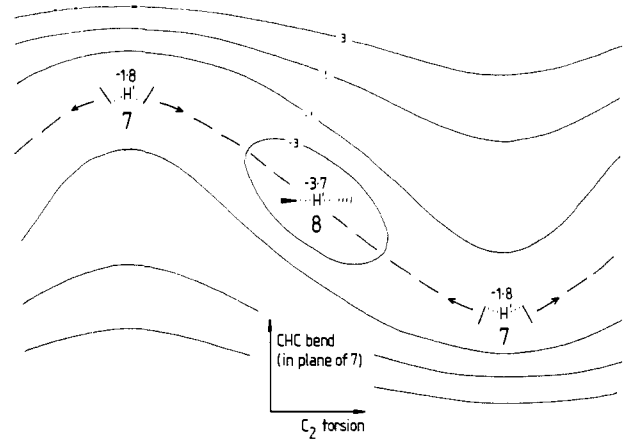

Figure 8. Schematic contour map of CH_3O^-/CH_2O transition structures (analogous to Figure 6a) at the semiempirical AM1 level.

that is slightly stabilized by 2e TS aromaticity.

Other work[11] has indicated that the semiempricial AM1 MO method[29] fails to predict 6e TS aromaticity of the type described above. Figure 8 shows the AM1 projection map for CH_3O^-/CH_2O analogous to Figure 6a. It is much simpler than Figure 6a and may be understood simply in terms of steric and electrostatic factors favoring **8** relative to **7**. There is no critical point on this surface corresponding to **5**.

Intrinsic Reaction Coordinates. In order to verify the topographical organization of critical points for each reaction surface depicted in Figures 5 and 6, the minimum energy path interconnecting each pair of adjacent critical points was determined within a particular symmetry constraint. Owing to the gentle curvatures and very low gradients along these surfaces, none of the methods[15,30] (linear, stabilized linear, quadratic, fourth-order Adams–Moulton predictor–coorector, and fourth-order Runge–Kutta methods) available in our version of the GAMESS program[16] proved to be efficient. Unless extremely small step sizes were employed, the algorithm would soon depart from the steepest descent path and would start to go uphill. To move from **6** to **7** (Figure 6a) in C_{2v} symmetry required about 200 path points.[31] The verification procedure was therefore exceedingly demanding of computational resources. The point marked by an asterisk in Figure 6 proved to be very troublesome; by the time the reaction path arrived at a structure having a CH'C angle equal to 180°, both the geometry and energy were appreciably different from the constrained optimized geometry at this point. These methods are therefore expensive and possibly misleading; this only serves to emphasize further the value of the approach we have described in this work. Koseki and Gordon[32] have recently shown how similar difficulties with IRC calculations on very flat PE surfaces may be overcome using a local quadratic approximation method.[33]

It was not possible to follow a path from **9** to **10** (Figure 6b) since the HTRC has the same symmetry (C_1) as the desired path between these critical points. The C_1 point group, of course, has only one irreducible representation, and so there does not exist any subspace in which the IRC path from **9** (a second-order saddle point) to **10** (a first-order saddle point) may be followed by the imposition of a suitable symmetry constraint. The direction of the initial step along the desired path is given by the CH'C bending normal coordinate whose vibrational wavenumber is $80i$ cm^{-1}, but

(25) Swain, C. G.; Wiles, R. A.; Bader, R. F. W. *J. Am. Chem. Soc.* **1961**, *83*, 1945.
(26) Olah, G. A.; Surya Prakash, G. D.; Williams, R. E.; Field, L. D.; Wade, K. *Hypercarbon Chemistry*; Wiley: New York, 1987; p 15.
(27) Stewart, R. *Oxidation Mechanisms*; Benjamin: New York, 1964; pp 18–26.
(28) Apin, A. E.; Williams, I. H. Manuscript in preparation.
(29) Dewar, M. J. S.; Zoebisch, E. G.; Healy, E. F.; Stewart, J. J. P. *J. Am. Chem. Soc.* **1985**, *107*, 3902.
(30) Garrett, B. C.; Redmon, M. J.; Steckler, R.; Truhlar, D. G.; Baldridge, K. K.; Bartol, D.; Schmidt, M. W.; Gordon, M. S. *J. Phys. Chem.* **1988**, *92*, 1476.
(31) The initial step away from **6** along the CH'C in-plane bending normal coordinate was chosen to reduce the total energy by 5×10^{-5} hartrees, and the stride length for subsequent steps was initially set to 0.02 amu$^{1/2}$ bohr. The stride was increased manually during the middle section of the IRC path between **6** and * but never exceeded 0.10 amu$^{1/2}$ bohr; the average stride length between **6** and * was 0.064 amu$^{1/2}$ bohr.
(32) Koseki, S.; Gordon, M. S. *J. Phys. Chem.* **1989**, *93*, 118.
(33) Page, M.; McIver, J. W. *J. Chem. Phys.* **1988**, *88*, 922.

the HTRC (of the same symmetry) has a vibrational wavenumber of $1183i$ cm^{-1}. Owing to the order of magnitude difference in the curvatures along these two directions, it was found that any finite step size along the desired eigenvector in rectilinear coordinates from **9** immediately misdirected the path down toward an undesired reactant-like structure instead of proceeding toward **10**. This is because there is only a single orthogonal trajectory from **9** to **10** but an infinite number of orthogonal trajectories from **9** to the CH_3O^-/CH_2O reagent minimum.

Conclusions

We have described the topographical features of the transition-state regions of the PE hypersurfaces for a pair of isoelectronic symmetrical hydride-transfer reactions calculated at the HF/3-21G level of ab initio MO theory. Undoubtedly the small size of the basis set employed and the neglect of electron-coorelation effects mean that the results of this work are not quantitatively reliable. Our purpose, however, was not to make a definitive study of the energetics and dynamics of these reactions per se; instead, our concern has been to examine these reacting systems, *as described by a particular theoretical model*, in order to demonstrate aspects of the complexity and subtlety of the topographical features that are possible for multidimensional reaction surfaces of even very "simple" organic reactions. The validity of our discussion would not be diminished in the slightest if it were to be shown that a particular topographical feature of one of these PE hypersurfaces was an artifact of an inadequate level of calculation.

Our strategy for topographical exploration is quite general. We have emphasized the importance of considering not only the *eigenvalues* of the Hessian matrix for each critical point on the PE hypersurface but also the corresponding *eigenvectors*, particularly the nature of any transition vector. The utility of the approach we have described will be greatest for reacting systems possessing elements of symmetry. However, it is worth pointing out that an efficient strategy for investigation of transition states for reactions *not* possessing symmetry may be to start with a symmetrical (perhaps unsubstituted) model reaction. Transition-state structural features, including geometrical parameters and Hessian matrix elements, may be obtained economically for a simpler symmetrical model and may provide invaluable initial guesses for studies of larger unsymmetrical reactions of interest.

We have shown how the curvature of a PE hypersurface along the reaction coordinate, and perhaps other coordinates of interest, may be rationalized qualitatively by means of the second-order Jahn–Teller effect.

We have characterized five new critical points (**3–6**, **9**) on the HF/3-21G reaction surfaces for $CH_3NH_2/CH_2NH_2^+$ and CH_3O^-/CH_2O. (Structures analogous to **3** and **4** are presumably also critical points on the $CH_3NH_2/CH_2NH_2^+$ surface.) We have argued that the geometries of these hydride-transfer transition structures may be understood as resulting from the interplay of three factors: steric interactions, electrostatic interactions, and the possibility of 2e or 6e transition-state σ-aromaticity.

Finally we note that the transition-state region of the CH_3O^-/CH_2O reaction surface contains no less than six distinct critical points within the range of chemically significant energies. Any treatment of reaction dynamics over such a surface would necessarily have to consider the properties of the whole transition-state region rather than just of a unique transition structure. Degenerate hydride-transfer reactions of the type considered in this work resemble the symmetrical heavy–light–heavy transition states that have been found to give the largest differences between conventional transition-state and variational transition-state treatments and for which quantum mechanical tunneling is important at geometries outside of the saddle-point region.[34] A quantitative theoretical study of the rates and mechanisms of these reactions would have to take these effects into consideration (cf. ref 35).

Registry No. CH_3NH_2, 74-89-5; $CH_2NH_2^+$, 34516-31-9; CH_3O^-, 3315-60-4; CH_2O, 50-00-0.

(34) Garrett, B. C.; Truhlar, D. G.; Wagner, A. F.; Dunning, T. H. *J. Chem. Phys.* **1983**, *78*, 4400. Bondi, D. K.; Connor, J. N. L.; Garrett, B. C.; Truhlar, D. G. *Ibid.* **1983**, *78*, 5981.

(35) Kreevoy, M. M.; Ostović, D.; Truhlar, D. G.; Garrett, B. C. *J. Phys. Chem.* **1986**, *90*, 3766.